Journal of Climate Change
ISSN 2395-7611 Volume 11 (2025) No. 4. pp. 390–409

https://doi.org/10.70917/jcc-2025-027
Article

Parametric Analysis of Thermal and Electrical Performance of Photovoltaic Thermal Systems Using Nano-Graphene Coolants and Enhanced Fin Design

Ehsan Baniasadi [1,*], Farzin Bahadori [1], Zahra Taheri [1] and Saffa Riffat [2]

[1] Department of Mechanical Engineering, Faculty of Engineering, University of Isfahan, Hezar Jerib Ave., Isfahan 81746-73441, Iran
[2] Department of Architecture and Built Environment, University of Nottingham, University Park, NG7 2JQ Nottingham, United Kingdom
* Corresponding author: e.baniasadi@eng.ui.ac.ir

Abstract: This study presents a comprehensive three-dimensional numerical simulation to assess the performance of a photovoltaic thermal (PVT) system utilizing nanofluids (NFs) and enhanced fin configurations. The system integrates a copper flat plate collector, where nanofluids circulate within heat absorber tubes, and rectangular fins are strategically arrayed to augment heat dissipation. The effects of fin dimensions, count, nanofluid concentration, flow rate, and solar intensity on the PVT's thermal and electrical performance are examined. Key findings illustrate that fin configuration, particularly the number of fins, significantly dictates the system's thermal management, with minimal impact from fin thickness. Optimal thermal behavior was observed with 0.5 wt% graphene nanoplatelet nanofluid at a mass flow rate of 0.1 kg/s, employing 400 fins. Analysis reveals that increasing the number of fins from 10 to 400 could enhance the thermal efficiency by approximately 18%, while reducing the overall system temperature by up to 7°C under peak solar conditions. Furthermore, the study indicates that an increase in solar radiation intensity from 800 to 1000 W/m2 reduces the electrical efficiency by about 2%, even though the electrical power output increases by 5%.

Keywords: photovoltaic thermal system; heat transfer enhancement; electrical efficiency; nanofluid

1. Introduction

PVTs are systems that simultaneously convert solar energy into electrical and thermal energy. Working fluid flowing in the absorber tubes reduces the solar collector temperature, improving the electrical efficiency (Ahmed et al., 2025) and power output (Khan et al., 2024). Hence, there is a close relationship between their thermal and electrical performances, which depend on various parameters, such as climatic conditions, fluid thermophysical properties, geometrical factors, and electrical characteristics (Hakimi, Baniasadi and Afshari, 2024).

Numerous researchers have conducted numerical and experimental investigations to assess the performance of PVTs. Sofiah et al. (2024) experimentally formulated and characterized *hexagonal boron nitride* (hBN)–water nanofluids, demonstrating that the nanoparticles yield significant enhancements in thermal conductivity, viscosity, and density behavior, which are critical for effective heat transfer in PVT systems. The authors identify an optimal concentration (0.5 vol%) that stabilizes the fluid and ensures superior cooling performance, leading to a controlled cell temperature and improved electrical output in the PVT setup. Oztürk et al. (2024) presented an integrated experimental investigation into three different PVT configurations, standard V-grooved, nano-enhanced V-grooved, and V-grooved with thermal energy storage, and evaluated them using energy, exergy, and sustainability metrics. The study demonstrates that nano-coating of absorber surfaces using graphene nanoparticles, as well as the

incorporation of phase change material for thermal storage, markedly improve both the thermal and electrical performance of the system while reducing waste exergy. Chandan et al. (2021) developed a steady-state three-dimensional numerical model to estimate the performance of glazed and unglazed PVT-FPC collectors. They fabricated PVT collectors and connected them in series to a flat plate collector (FPC). The peak value of η_{th} of the unglazed collector was 25%, while η_{th} of the FPC collector was 35%. Besides, the peak temperature of the outlet water for the glazed and unglazed PVT-FPC system was 65-67 ºC and 60-63 ºC, respectively. Maadi et al. (2021) evaluated the performance of a PVT system by inserting wavy strips and using Al_2O_3/water NF. They reported 3.5% and 12.06% improvement in η_{elec} and η_{th}, respectively, in comparison with a conventional PVT. Khodadadi et al. (2021) modified a PVT with a linear Fresnel reflector (LFR) by employing phase change material (PCM). They examined the impact of $\dot{m}$ and the utilization of Al_2O_3/water NF and PCM on the collector performance, and demonstrated that the system thermal output is enhanced by adding nanoparticles to water and PCM.

Arifin et al. (2022) considered the influences of TiO_2/water NF on the performance of a PVT system numerically and experimentally. It was found that T_{cell} is diminished with the use of NF. Also, η_{elec} of the NF-based and water-based systems was 13.04% and 12.22%, respectively. Sreekumar et al. (2022) conducted three-dimensional numerical simulations to explore the impact of a Mxene/water NF on η_{th} and CO_2 emission rate of a PVT system. The results revealed that the NF with φ = 0.2 wt% improves η_{elec} and η_{th} of the PVT by 3.5% and 17%, respectively, compared to those of a water-based system. Using NF enhances the heat transfer coefficient by 21.42% compared to water, declining the PVT outlet temperature by about 10%. They demonstrated a 4.5-14.5% reduction in NF-based PVT size compared to the conventional one. Hai et al. (2022) simulated a PVT system with a copper tube containing Al_2O_3/water NF. The system consisted of some tube-connected elliptical fins placed in a PCM-filled chamber under the panel. It was found that the fins with a central hole reduce the T_{out} of NF and the PVT temperature. Maadi et al. (2019) developed a three-dimensional thermal-optical model to evaluate the performance of a glazed PVT module. They reported that the greenhouse considerations have a pivotal impact on η_{th}, particularly when SRI is low; however, its effect on η_{elec} can be ignored. It was also demonstrated that an enhancement in the number of tubes and bonding alters the temperature profile of the PV cells significantly.

Al-Shamani et al. (2018) assessed the impact of ZnO/water, SiO_2/water, and CuO/water NFs on the electrical and η_{th} of a PVT system and T_{out} of the fluid numerically and experimentally. The results revealed that the optimal number of rectangular absorber tubes is 11. The optimal value of $\dot{m}$ corresponding to the maximum overall efficiency was 0.03 kg/s, and the best performance was related to SiO_2/water NF. Nasrin et al. (2018) proposed a novel Multi-Walled Carbon Nanotubes (MWCNT)/water NF-based PVT module for different radiation levels ranging from 200 W m^{-2} to 1000 W m^{-2}, the weight fraction range of 0-1%, and the volumetric flow rate was 0.5 L/min. The PVT overall efficiency was 89.2% and 87.65% obtained from numerical and experimental investigations, respectively, when SRI was 1000 W/m^2. Shehadeh et al. (2019) examined the influence of weather conditions on the PV cell ratio to obtain the maximum overall thermal energy. They showed that the maximum overall thermal energy is obtained for a variable PVT coverage ratio annually. They observed that if the PVT surface is covered with PV cells, the system becomes suitable for low-temperature applications (25-40°C).
Rajvikram and Sivasankar (2019) experimentally assessed the impact of a PCM and an external finned heatsink to enhance the thermal conductivity (K) of the PCM. The researchers considered four cases and concluded that using the PVT with PCM and the heatsink decreases operating temperature. Lari and Sahin (2017) designed an NF-based PVT system to meet the electrical needs of a residential building under the climatic conditions of Dhahran in Saudi Arabia. They reached an 8.5% enhancement in the electrical output and a 13% increase in the thermal output of their proposed PVT system compared to the conventional one. Abdallah et al. (2018) experimentally evaluated the performance of a PVT system using Al_2O_3/water NF as a working fluid. They demonstrated that the use of NF enhances the combined performance of PVT by 74% and 56% when the NF volume fraction is 0.1%. They also found that the changes in the produced electricity have the same trend as SRI, and the maximum produced electricity occurs at the maximum solar radiation.

Al-Waeli et al. (2017) used SiC/water NF as a coolant in a PVT system and observed that K is enhanced by 8.2% by adding 3 wt% nanoparticles to water. Their results determined that the overall efficiency of the PVT system is about 88.9% greater than that of the separate PVT system. Alktranee et al. (2024) examined the cooling of a PVT hybrid system by using CuO/water and Fe_2O_3/water NFs with different volume fractions and demonstrated that when φ = 0.3%, the electrical power output is enhanced and η_{elec} is improved by 9.21% and 10.30%, respectively. Also, the increase in temperature absorption augmented η_{th} by 43.3%. Sreekumar et al. (2024) assessed the effect of cooling PVT systems by C-

dot/water and MXene/water hybrid NFs. Using the hybrid NF, they obtained η_{th} of a PVT of about 57.45%, which was 9.45% higher than water. η_{elec} of the system with a hybrid NF was 17.98%. Alhamayani (2024) evaluated a PVT system using Al_2O_3/water, CuO/water, and TiO_2/water NFs with different volume fractions and revealed that CuO/water NF with φ = 4% performs best and improves η_{th} and η_{elec} by 79.2% and 16.7%, respectively. Table 1 compares the main findings of the previous works.

Table 1. Summary of the previous works conducted on PVT systems.

Subject	Highlights	Ref.
Estimation of the performance of glazed and unglazed PVT-FPC collectors	- The maximum values of η_{th} for the unglazed and glazed collectors were 25% and 35%, respectively. - The maximum temperature of the outlet water for the glazed and unglazed PVT-FPC system was 65-67 ºC and 60-63 ºC, respectively	(Chandan et al., 2021)
Evaluation of the performance of a PVT system by inserting wavy strips and using Al_2O_3/water NF	- The proposed PVT system showed 3.5% and 12.06% improvement in η_{elec} and η_{th}, respectively, in comparison with a conventional PVT.	(Maadi et al., 2021)
Influence assessment of TiO_2/water NF on the performance of a PVT system numerically and experimentally.	- T_{cell} was reduced with the use of NF. - η_{elec} of the NF-based and water-based systems was 13.04% and 12.22%, respectively	(Arifin et al., 2022)
Simulation of a PVT system with a copper tube containing Al_2O_3/water NF.	- The fins with a central hole reduced the T_{out} of NF and the PVT temperature.	(Hai et al., 2022)
Assessment of the impact of ZnO/water, SiO_2/water, and CuO/water NFs on the performance a PVT system	- The optimal number of rectangular absorber tubes was 11. - The optimal value of $\dot{m}$ corresponding to the maximum overall efficiency was 0.03 kg/s.	(Al-Shamani et al., 2018)
Examination of the impact of a PCM and an external finned heatsink on the performance of a PVT system	- The PVT with PCM and the heatsink shows a decrease in its operating temperature.	(Rajvikram and Sivasankar, 2019)
Design of an NF-based PVT system	- An 8.5% enhancement in the electrical output and a 13% increase in the thermal output of the proposed PVT system were reported compared to the conventional one.	(Lari and Sahin, 2017)
Cooling of a PVT hybrid system by using CuO/water and Fe_2O_3/water NFs	- When φ = 0.3%, the electrical power output and η_{elec} were improved by 9.21% and 10.30%, respectively. - The increase in temperature absorption enhanced η_{th} by 43.3%.	(Alktranee et al., 2024)
Subject	Highlights	Ref.
Estimation of the performance of glazed and unglazed PVT-FPC collectors	- The maximum values of η_{th} for the unglazed and glazed collectors were 25% and 35%, respectively. - The maximum temperature of the outlet water for the glazed and unglazed PVT-FPC system was 65-67 ºC and 60-63 ºC, respectively	(Chandan et al., 2021)

Evaluation of the performance of a PVT system by inserting wavy strips and using Al_2O_3/water NF	- The proposed PVT system showed 3.5% and 12.06% improvement in η_{elec} and η_{th}, respectively, in comparison with a conventional PVT.	(Maadi et al., 2021)
Influence assessment of TiO_2/water NF on the performance of a PVT system numerically and experimentally.	- T_{cell} was reduced with the use of NF. - η_{elec} of the NF-based and water-based systems was 13.04% and 12.22%, respectively	(Arifin et al., 2022)
Simulation of a PVT system with a copper tube containing Al_2O_3/water NF.	- The fins with a central hole reduced the T_{out} of NF and the PVT temperature.	(Hai et al., 2022)
Assessment of the impact of ZnO/water, SiO_2/water, and CuO/water NFs on the performance a PVT system	- The optimal number of rectangular absorber tubes was 11. - The optimal value of $\dot{m}$ corresponding to the maximum overall efficiency was 0.03 kg/s.	(Al-Shamani et al., 2018)
Examination of the impact of a PCM and an external finned heatsink on the performance of a PVT system	- The PVT with PCM and the heatsink shows a decrease in its operating temperature.	(Rajvikram and Sivasankar, 2019)
Design of an NF-based PVT system	- An 8.5% enhancement in the electrical output and a 13% increase in the thermal output of the proposed PVT system were reported compared to the conventional one.	(Lari and Sahin, 2017)
Cooling of a PVT hybrid system by using CuO/water and Fe_2O_3/water NFs	- When φ = 0.3%, the electrical power output and η_{elec} were improved by 9.21% and 10.30%, respectively. - The increase in temperature absorption enhanced η_{th} by 43.3%.	(Alktranee et al., 2024)
Subject	Highlights	Ref.
Estimation of the performance of glazed and unglazed PVT-FPC collectors	- The maximum values of η_{th} for the unglazed and glazed collectors were 25% and 35%, respectively. - The maximum temperature of the outlet water for the glazed and unglazed PVT-FPC system was 65-67 ºC and 60-63 ºC, respectively	(Chandan et al., 2021)
Evaluation of the performance of a PVT system by inserting wavy strips and using Al_2O_3/water NF	- The proposed PVT system showed 3.5% and 12.06% improvement in η_{elec} and η_{th}, respectively, in comparison with a conventional PVT.	(Maadi et al., 2021)
Influence assessment of TiO_2/water NF on the performance of a PVT system numerically and experimentally.	- T_{cell} was reduced with the use of NF. - η_{elec} of the NF-based and water-based systems was 13.04% and 12.22%, respectively	(Arifin et al., 2022)
Simulation of a PVT system with a copper tube containing Al_2O_3/water NF.	- The fins with a central hole reduced the T_{out} of NF and the PVT temperature.	(Hai et al., 2022)
Assessment of the impact of ZnO/water, SiO_2/water, and CuO/water NFs on the performance a PVT system	- The optimal number of rectangular absorber tubes was 11. - The optimal value of $\dot{m}$ corresponding to the maximum overall efficiency was 0.03 kg/s.	(Al-Shamani et al., 2018)

Examination of the impact of a PCM and an external finned heatsink on the performance of a PVT system	- The PVT with PCM and the heatsink shows a decrease in its operating temperature.	(Rajvikram and Sivasankar, 2019)
Design of an NF-based PVT system	- An 8.5% enhancement in the electrical output and a 13% increase in the thermal output of the proposed PVT system were reported compared to the conventional one.	(Lari and Sahin, 2017)
Cooling of a PVT hybrid system by using CuO/water and Fe_2O_3/water NFs	- When φ = 0.3%, the electrical power output and η_{elec} were improved by 9.21% and 10.30%, respectively. - The increase in temperature absorption enhanced η_{th} by 43.3%.	(Alktranee et al., 2024)

This study assesses the effectiveness of a PVT system that employs NFs and copper straight absorber tubes. The research primarily contributes in two significant ways: first, it introduces rectangular fins positioned beneath the absorber tubes to improve heat transfer, and second, it explores the application of NFs as working fluids. The investigation focuses on three distinct types of NFs, i.e., graphene nanoplatelets/water, Al2O3/water, and SiC/water, to analyze their impact on the thermophysical properties and overall performance of the PVT system. The main goal is to enhance the heat transfer rate and boost output power by integrating NFs and fin structures into the system. These quantitative insights into the thermodynamic behavior of the system under varied operational scenarios contribute significantly to the field of solar energy conversion, highlighting the importance of detailed component and fluid dynamic analysis in the design and development of high-performance PVT systems. The rest of the paper is organized as follows: Section 2 outlines the problem statement, while Section 3 presents the governing equations and numerical methods. Sections 4 and 5 cover the grid study and verification of the numerical results, respectively. Section 6 discusses the findings, and finally, Section 7 offers the concluding remarks.

2. System description

Figure 1 demonstrates that the system has thermal symmetry for each tube, and the temperature characteristics are repeated alternately. Hence, the results obtained for the whole system are the same as those achieved for a single tube. The geometry includes a glass cover, ethylene vinyl acetate (EVA) layer, PV cells, heat absorber, tube, welds, and fins. Tables 2 and 3 present the dimensions and properties of the materials used in the system. Figure 2 illustrates a schematic of the PVT system. The system uses fins with pitches varying from 10 to 800. The reference model has 400 fins.

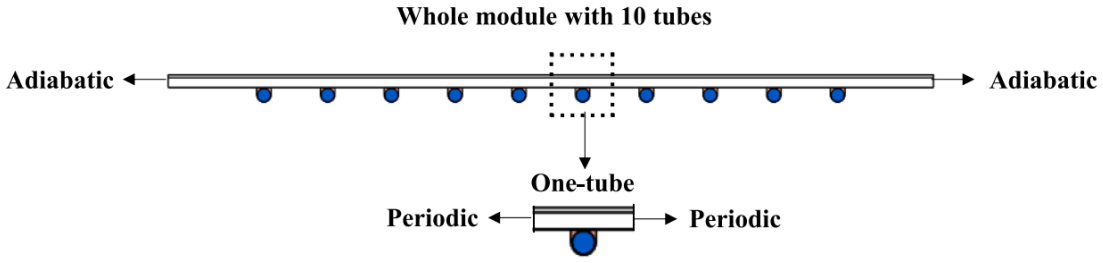

Figure 1. Schematic of the PVT module with 10 and single tubes (Maadi et al., 2019).

Table 2. Dimensions of the PVT system

Component	Size (mm)
The glass cover thickness	3
EVA layer thickness	1.5
Solar cell thickness (Pc-Si)	1.2
The heat absorber thickness	2

The inner diameter of the tube	8
The thickness of the fins	2, 1.5, 1
The plate length	2000
The plate width	100
The tube length	2000

Table 3. Properties of different layers of the PVT system (Maadi et al., 2019).

Material	Density (kg/m³)	Heat capacity (J/kg K)	K (W/m K)
Glass	2500	750	1.4
PV cells	2330	700	148
EVA	960	2090	0.35
Absorber, tube, and welding (copper)	8954	385	310

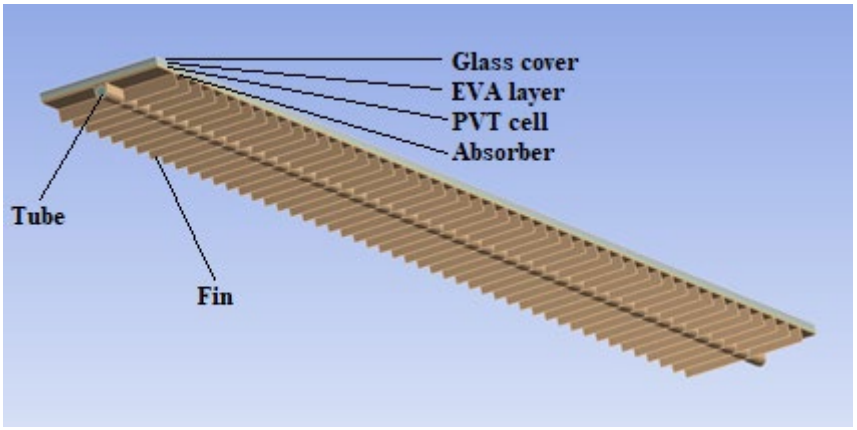

Figure 2. Three-dimensional geometry of a single-tube PVT with fins under the absorber plate.

3. Governing equations and numerical solution method

Considering the PVT system as a control volume, the governing equations are as follows (Hasan et al., 2022):

Continuity equation:

$$\frac{\partial u}{\partial x}+\frac{\partial v}{\partial y}+\frac{\partial w}{\partial z}=0 \tag{1}$$

Momentum equation:

$$\rho\left(u\frac{\partial u}{\partial x}+v\frac{\partial u}{\partial y}+w\frac{\partial u}{\partial z}\right)=\rho g_x-\frac{\partial p}{\partial x}+\mu\left(\frac{\partial^2 u}{\partial x^2}+\frac{\partial^2 u}{\partial y^2}+\frac{\partial^2 u}{\partial z^2}\right) \tag{2}$$

$$\rho\left(u\frac{\partial v}{\partial x}+v\frac{\partial v}{\partial y}+w\frac{\partial v}{\partial z}\right)=\rho g_y-\frac{\partial p}{\partial y}+\mu\left(\frac{\partial^2 v}{\partial x^2}+\frac{\partial^2 v}{\partial y^2}+\frac{\partial^2 v}{\partial z^2}\right) \tag{3}$$

$$\rho\left(u\frac{\partial w}{\partial x}+v\frac{\partial w}{\partial y}+w\frac{\partial w}{\partial z}\right)=\rho g_z-\frac{\partial p}{\partial z}+\mu\left(\frac{\partial^2 w}{\partial x^2}+\frac{\partial^2 w}{\partial y^2}+\frac{\partial^2 w}{\partial z^2}\right) \tag{4}$$

Energy equation:

$$\rho C_p\left(u\frac{\partial T}{\partial x}+v\frac{\partial T}{\partial y}+w\frac{\partial T}{\partial z}\right)=K\left(\frac{\partial^2 T}{\partial x^2}+\frac{\partial^2 T}{\partial y^2}+\frac{\partial^2 T}{\partial z^2}\right)+\Phi \tag{5}$$

$$\Phi=\mu\left[2\left(\frac{\partial u}{\partial x}\right)^2+2\left(\frac{\partial v}{\partial y}\right)^2+2\left(\frac{\partial w}{\partial z}\right)^2+\left(\frac{\partial v}{\partial x}+\frac{\partial u}{\partial y}\right)^2+\left(\frac{\partial w}{\partial y}+\frac{\partial v}{\partial z}\right)^2+\left(\frac{\partial u}{\partial z}+\frac{\partial w}{\partial x}\right)^2\right] \tag{6}$$

The pressure-based finite volume method (FVM) is used to solve governing equations by employing the ANSYS FLUENT 19 software. Velocity and pressure fields are coupled using the SIMPLE scheme. Also, the second-order upwind method is utilized to discretize the momentum and energy equations. The following assumptions and boundary conditions are used to perform the simulations:

• The system is completely insulated.

• The bottom of the system is subject to convective heat transfer.
• The panel's upper surface is exposed to SRI = 1000 W/m^2 while convective heat transfer is ignored.
• The inlet temperature of the fluid is 25 ºC.
• The mass flow rate is kept constant.
• The cooling fluid pressure is zero at the tube outlet.
• The properties of solid components do not depend on the temperature.
• Solar radiation is perpendicular to the system.
• Radiation losses to the environment are negligible.
• The fluid flow is laminar, steady, and uniform.
• The properties of water and NFs are calculated based on the inlet temperature.

The convective heat transfer coefficient on the outer surfaces for a velocity less than 5 m/s is calculated using the following equation (Maadi et al., 2019):

$$h = 5.7 + 3.8\,V_{wind} \tag{7}$$

where V_{wind} is the wind speed. It should be pointed out that h reduces by enhancing the number of fins until it reaches a certain value; however, in the present simulations, h is assumed to be constant and depends only on V_{wind}.

Total, η_{elec}, and η_{th} can be used to measure the performance of a PVT system. The useful thermal energy is calculated using the following equation (Abdallah et al., 2018):

$$Q_u = \dot{m}C_p(T_{out} - T_{in}) \tag{8}$$

where C_p is the specific heat capacity, T_{out} is the fluid outlet temperature, and T_{in} is the fluid inlet temperature.

The thermal efficiency of the system is determined as follows (Abdallah et al., 2018):

$$\eta_{th} = \frac{Q_u}{G \times A_c} \tag{9}$$

where G is the incident solar radiation perpendicular to the surface and A_c is the collector surface area.

The electrical efficiency is estimated using Eq. 10 (Sreekumar et al., 2024):

$$\eta_{elec} = \eta_r[1 - \beta(T_{cell} - T_r)] \tag{10}$$

where T_r and η_r are the temperature and efficiency of the PV cell in reference conditions, i.e., 25 ºC and 1000 W/m^2. T_{cell} is the temperature of the PV cell in which the efficiency is calculated and β is the temperature coefficient of the PV cell (for crystalline silicon cells β = - 0.0045).

The electric power output is computed as follows (Yazdanifard, Ebrahimnia-Bajestan and Ameri, 2016):

$$E_{pv} = \eta_{elec} \times A_{pv} \times G \tag{11}$$

where A_{pv} is the surface area of the PVT module.

The total efficiency is (Abdallah et al., 2018):

$$\eta_{tot} = \eta_{th} \times \eta_{elec} \tag{12}$$

4. Grid independence study

The computational domain should be discretized to do numerical simulations by generating appropriate grids. The mechanical workbench part of the ANSYS FLUENT software is used to generate the grids. Since a large number of grid elements results in solution errors and too fine grids lead to high computational costs, it is crucial to provide an optimal grid. Since the size and quality of the grid affect the solution results, it is pivotal to perform the grid study. Three grids with 237014, 502249, and 771034 elements are employed to estimate the amounts of T_{out} and T_{cell} (Table 4). Steady-state numerical simulations are performed for the input heat flux of 1000 W/m^2, the inlet water temperature of 298 K, and the total input ṁ of 0.1 kg/s when the number of absorber tubes is 1. Table 4 demonstrates that the difference between the results obtained from the grids with 502249 and 771034 elements is small, indicating that the grid with 502249 elements can be used for further simulations. Figure 3 illustrates the computational grid used.

Table 4. The PVT outlet temperature and PV cell for different grid sizes.

Number of elements	T_{cell}	T_{out}
237014	303.86	310.70
502249	304.10	311.31
771034	304.28	311.23

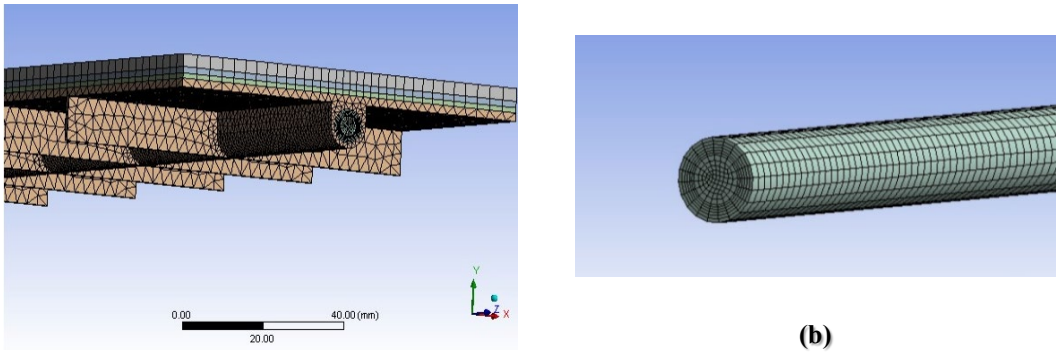

Figure 3. Computational domain of (a) PVT assembly, (b) heat transfer fluid conduit.

5. Validation of the computational model

To validate the present numerical results, T_{out} and T_{cell} are calculated and compared with the numerical results of Hasan et al. (2022) and Yazdanifard et al. (2016), who examined the performance of a flat plate PVT collector with a copper absorber tube (Figure 4a) cooled by water. The glass cover thickness is 4 mm, the insulation thickness is 50 mm, and the diameter and thickness of the tube are 8 mm and 1.2 mm, respectively.

Figures 4b and 4c demonstrate that the present results are in good agreement with those reported by Hasan et al. (2022) and Yazdanifard et al. (2016). The maximum error for T_{out} is 0.29%, and the maximum error for T_{cell} is 0.58%.

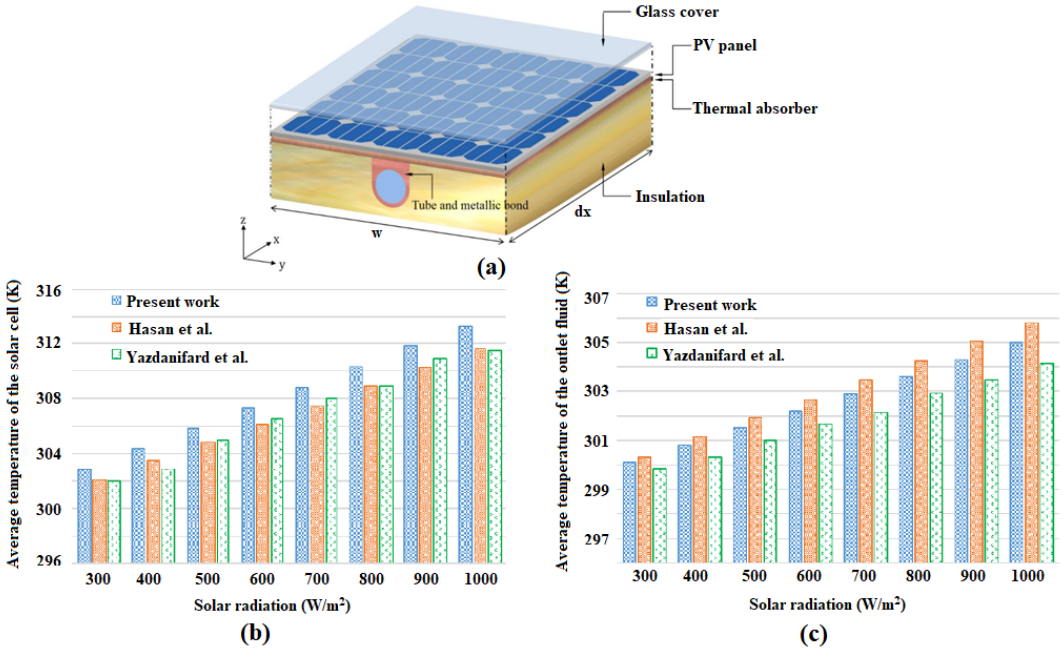

Figure 4. Validation: (a) Schematic of the PVT (Yazdanifard, Ebrahimnia-Bajestan and Ameri, 2016), (b) T_{out} versus solar radiation, and (c) T_{cell} as a function of solar radiation.

6. Results and discussion

6.1. Effect of fin thickness

Table 5 shows the effect of fin thickness on PVT performance for low and high $\dot{m}$ of 0.05 and 0.1 kg/s. It is observed that there is no significant change in the temperature of the outlet fluid and PVT surface by enhancing the fin thickness. This is due to the constant value of convection surface area because the increase in the area of the side surfaces can be ignored compared to the total surface of the absorber and fins. Thus, the fin thickness of 1 mm is selected for the PVT system.

Table 5. Effect of the thicknesses of fins on PVT performance in different flow rates.

	Fin thickness (mm)			Fin thickness (mm)		
	2	1.5	1	2	1.5	1
$\dot{m}$ (kg/s)	0.05			0.1		
T_{out} (K)	302.37	302.38	302.4	300.82	300.81	300.82
T_{cell} (K)	306.86	306.9	306.98	305.27	305.27	305.34
η_{elec} (%)	14.4	14.4	14.39	14.51	14.51	14.5
η_{th} (%)	45.67	45.77	45.98	58.94	58.93	58.94
η_{tot} (%)	60.07	60.17	60.37	73.45	73.44	73.44

6.2. Effect of the number of fins

In this section, the effect of the number of fins with a constant thickness of 1 mm on T_{out}, the difference between T_{in}, T_{out}, T_{cell}, η_{th}, η_{elec}, and η_{tot} of the PVT system is investigated (Figure 5). Two amounts of $\dot{m}$, i.e., 0.05 and 0.1 kg/s are considered, and the number of fins is 10, 20, 30, 40, 50, 75, 100, 200, 300, 400, 500, and 800. Figs. 5a and 5b show the variations of T_{out} and PVT temperature in terms of the number of fins, respectively. T_{out} is reduced with the number of fins for both values of $\dot{m}$; however, this reduction is greater for a low $\dot{m}$. This is due to a greater heat transfer area and more heat transfer from the system to the surroundings through the fins. By improving heat dissipation through a greater surface area for conduction and convection, adding fins to the system lowers the panel temperature. In order to improve thermal management and avoid localized hotspots, more fins offer more channels for heat to move away from the PV panel. The panel is more effectively cooled by the more efficient transmission of heat to the surrounding air made possible by the larger surface area. At a lower $\dot{m}$, the effect of fins on heat transfer and temperature reduction is higher because less heat is removed from the system by the fluid. The maximum temperature of the outlet fluid (304.15 K) corresponds to the fin number of 10 and $\dot{m}$ = 0.05 kg/s and the minimum one (300.28 K) corresponds to the fin number of 800, and $\dot{m}$ = 0.1 kg/s. The highest temperature of the PVT (311.17 K) corresponds to the fin number of 10 and $\dot{m}$ = 0.05 kg/s, and the lowest one (303.81 K) corresponds to the fin number of 800 and $\dot{m}$ = kg/s. Figure 5c shows the changes in η_{th} of the system as a function of the number of fins. In both values of $\dot{m}$, $\eta_{th}$is diminished with the number of fins. This is due to the reduction in T_{out}, according to Eq. 9, because all parameters are constant except for the temperature. The maximum η_{th} of the system (76.28%) corresponds to the fin number of 10 and $\dot{m}$ = 0.1 kg/s and the minimum one (35.53%) is related to the fin number of 800, and $\dot{m}$ = 0.05 kg/s. Figure 5d depicts the changes in $\eta_{elec}$of the system versus the number of fins. For both values of $\dot{m}$, the electrical efficiency is improved with the number of fins. This improvement is greater for a low $\dot{m}$. According to Eq. 10, the electrical efficiency is reduced by decreasing the PVT temperature. The maximum electrical efficiency (14.61%) corresponds to $\dot{m}$ = 0.1 kg/s when the number of fins is 800, and the minimum one (14.11%) is related to $\dot{m}$ = 0.05 kg/s. For a constant fin number, the system with a higher $\dot{m}$ has more electrical efficiency. Figure 5e illustrates the changes in the output power of the system versus the number of fins. Due to the decrease in the PVT temperature and the subsequent enhancement in the electrical efficiency, the system output power is improved. As the number of fins is enhanced, the system output power enhancement is higher for a low $\dot{m}$. Lowering the temperature with improved cooling immediately boosts power output since PV cells' electrical efficiency drops as the temperature rises. More fins also improve airflow dynamics and increase the surface area available for heat exchange, both of which enhance cooling efficiency. The total electrical power generated by the PVT system rises noticeably as a consequence of the cells producing more voltage and current as a result of the temperature drop. The maximum output power (1.146 W/m^2) corresponds to $\dot{m}$ = 0.1 kg/s when the number of fins is 800, and the minimum (1.141 W/m^2) is related to $\dot{m}$ = 0.05 kg/s when the number of fins is 10. Figure 5f depicts the changes in η_{tot} of the system in terms of the number of fins for both values of $\dot{m}$. The maximum η_{tot} (90.6%) corresponds to $\dot{m}$ = 0.1

kg/s when the number of fins is 10 and the minimum one (50.07%) corresponds to ṁ = 0.05 kg/s when the number of fins is 800.

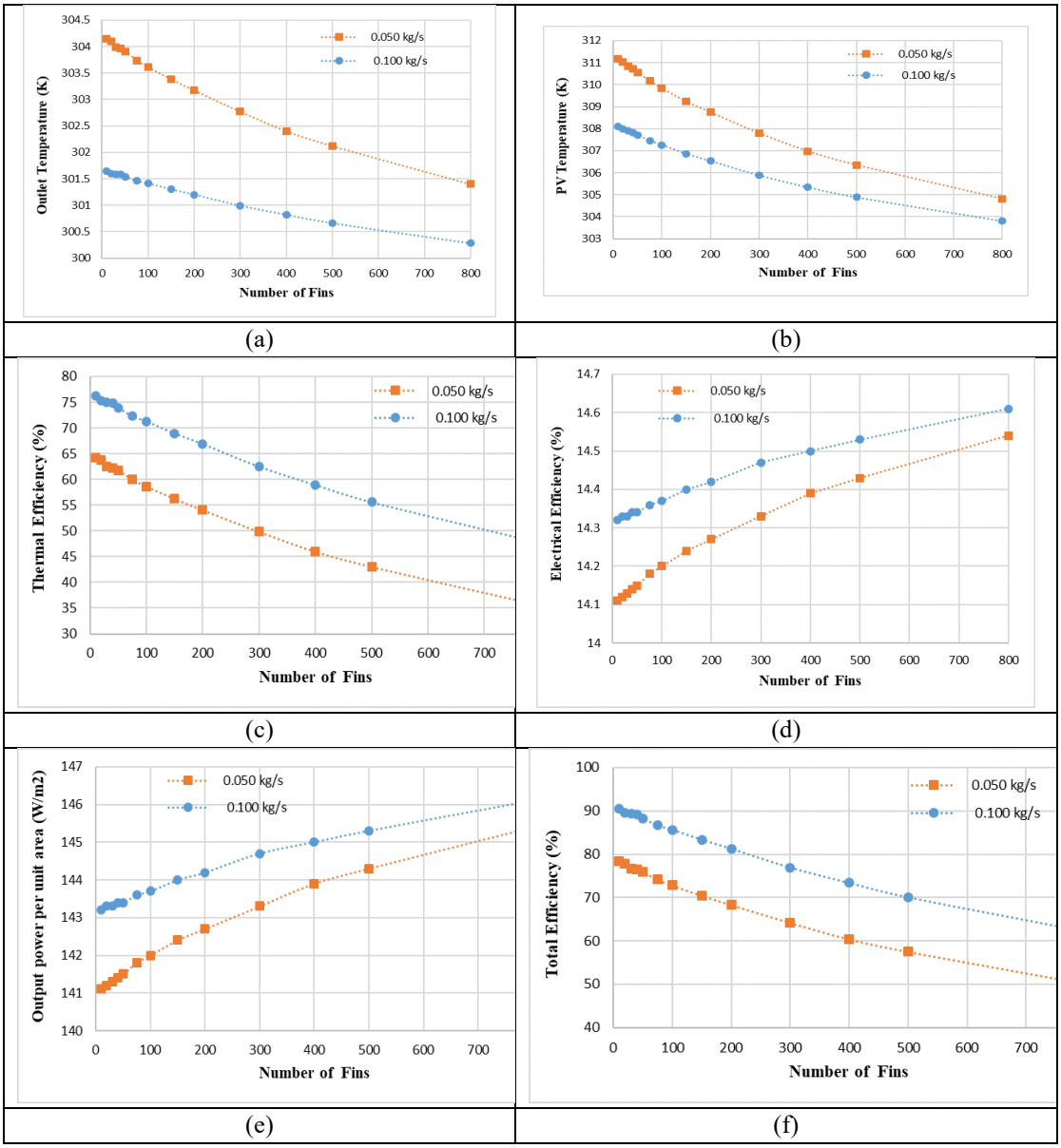

Figure 5. Effect of the number of fins on (a) T_{out}, (b) PVT temperature, (c) thermal efficiency η_{th}, (d) electrical efficiency η_{elec}, (e) the output power per unit area, and (f) total efficiency η_{tot}.

6.3. Effect of concentration, mass flow rate, and type of nanofluid

In this section, the performance of the PVT system is examined for three NFs with various values of φ by presenting T_{out}, PVT temperature, η_{th}, η_{elec}, output power per unit area, and η_{tot} for three amounts of ṁ (0.025, 0.05, and 0.1 kg/s). Figure 6a,b, and c illustrate T_{out} of the NF in terms of φ for alumina/water, GNP/water, and SiC/water NFs, respectively. For a given amount of φ, the maximum values of the outlet fluid temperature correspond to the minimum ṁ and the minimum ones correspond to the maximum ṁ. For all amounts of ṁ, T_{out} is enhanced with φ; however, this increase is greater for lower values of ṁ. Heat capacity reduction enhances the NF temperature by augmenting its φ. Besides, an increase in the dynamic viscosity weakens the movement of the fluid at a constant ṁ and thus, enhances the opportunity for heat exchange between the fluid and the absorber. In other words, the dynamic viscosity increases T_{out} by enhancing φ. Also, increasing ṁ reduces T_{out}. Because a larger φ improves the fluid's thermal conductivity and heat capacity, increasing φ in the system boosts the nanofluid's output temperature. As the nanofluid passes through the cooling channels, its enhanced

thermal characteristic enables it to absorb and transfer more heat from the PVT panel. Consequently, more thermal energy is carried away by the fluid exiting the system (output), raising the outlet temperature. This helps to maintain lower PV cell temperatures and increase overall system efficiency, even if it means the fluid leaves the panel hotter. It also reflects more efficient heat extraction from the panel. For alumina/water NF, the maximum T_{out} (314.62 K) corresponds to $\dot{m}$ = 0.025 kg/s and φ = 1 wt%, and the minimum one (301.68 K) corresponds to $\dot{m}$ = 0.1 kg/s when φ is 0.01 wt%. For GNP/water NF, the maximum T_{out} (316.83 K) corresponds to $\dot{m}$ = 0.025 kg/s and φ = 1 wt%, and the minimum one (301.68 K) corresponds to $\dot{m}$ = 0.1 kg/s when φ is 0.01 wt%. For SiC/water NF, the maximum T_{out} (315.29 K) corresponds to $\dot{m}$ = 0.025 kg/s and φ = 1 wt%, and the minimum one (301.68 K) corresponds to $\dot{m}$ = 0.1 kg/s when φ is 0.01 wt%.

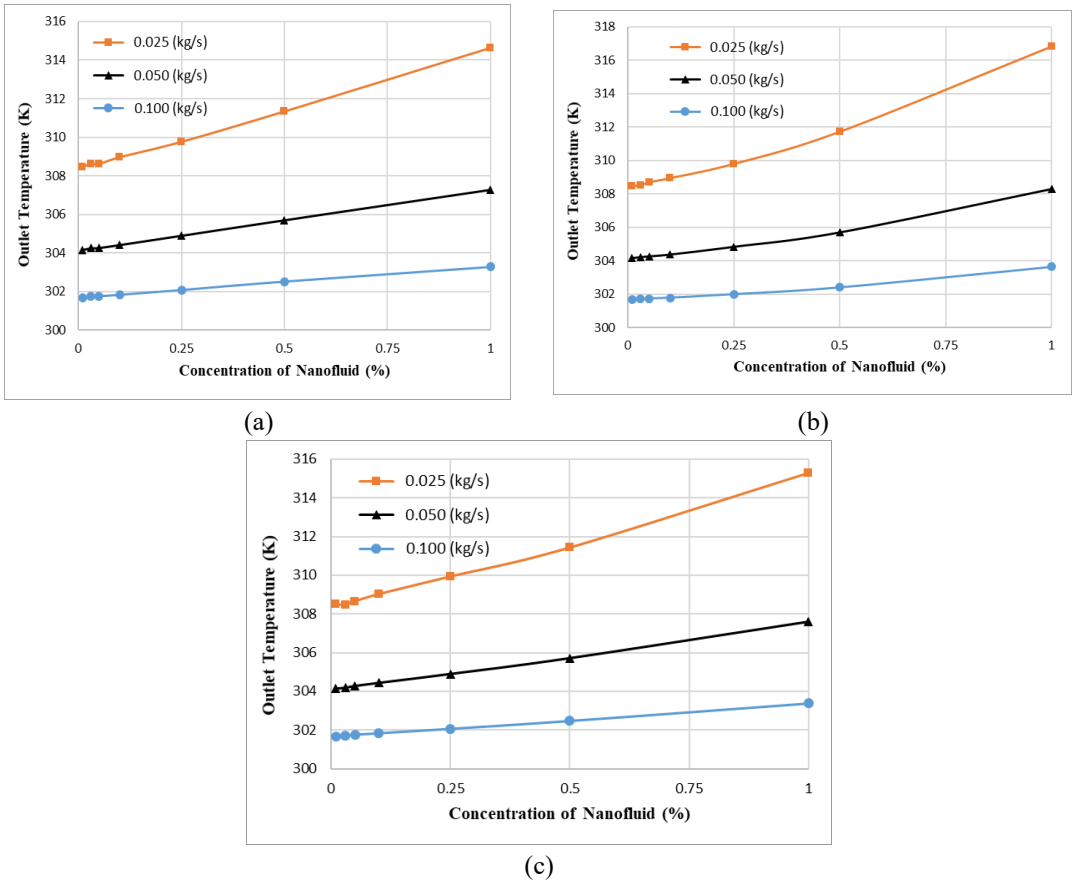

Figure 6. Effect of φ on T_{out} for different values of $\dot{m}$: (a) alumina/water, (b) GNP/water, and (c) SiC/water.

Figure 7 demonstrates the changes in the η_{th} of the PVT versus the weight concentration of the NFs for different amounts of $\dot{m}$. With the increase in φ, η_{th} is reduced, which is valid for all values of $\dot{m}$. This is due to the reduction of the NF heat capacity by enhancing φ (Eq. 9). On the other hand, the lower $\dot{m}$, the lower the corresponding η_{th} because despite the large inlet and T_{out} difference, less NF enters the system. In other words, the heat capacity reduction trend overcomes T_{out} enhancement, diminishing η_{th}. This can also be expressed that the specific heat capacity remains unchanged at a constant φ. As $\dot{m}$ is enhanced, η_{th} is improved, indicating that higher values of $\dot{m}$ due to the presence of more fluid takes more heat from the PVT per unit of time. Figure 7a illustrates that the maximum η_{th} (76.29%) corresponds to $\dot{m}$ = 0.1 kg/s when the alumina/water concentration is 0.01 wt% and the minimum one (46.2%) is related to $\dot{m}$ = 0.025 kg/s and a concentration of 1 wt%. Figure 7b shows that the maximum η_{th} (76.27%) corresponds to $\dot{m}$ = 0.1 kg/s when the GNP/water concentration is 0.01 wt% and the minimum one (44.73%) is related to $\dot{m}$ = 0.025 kg/s and a concentration of 1 wt%. Figure 7c demonstrates that the maximum η_{th} (76.27%) corresponds to $\dot{m}$ = 0.1 kg/s when the SiC/water concentration is 0.01 wt% and the minimum one (45.61%) is related to $\dot{m}$ = 0.025 kg/s and φ = 1 wt%.

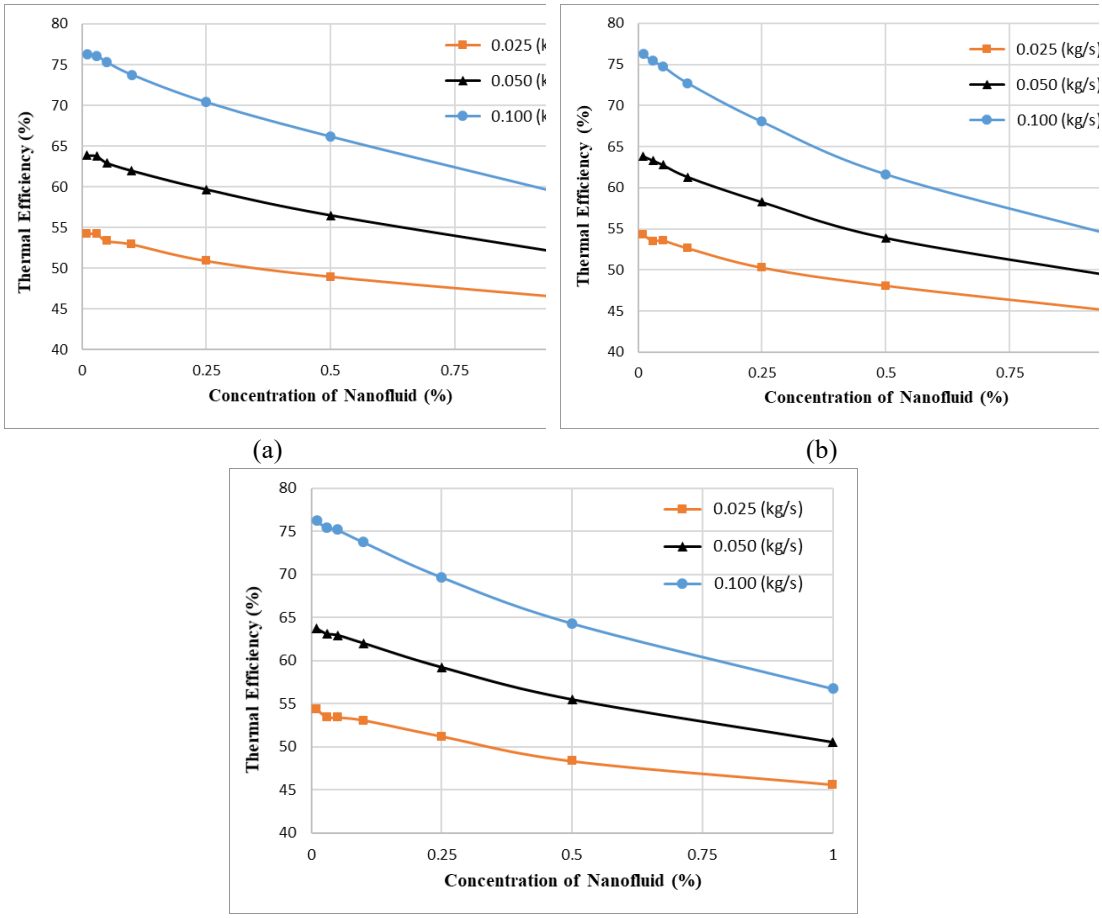

Figure 7. Effect of φ on η_{th} of the PVT for different amounts of ṁ: (a) alumina/water, (b) GNP/water, and (c) SiC/water.

Figure 8 depicts the PVT temperature changes versus the weight concentration of the NFs for three values of ṁ: 0.025, 0.05, and 0.1 kg/s. The PVT temperature is not reduced by enhancing φ. For a lower ṁ, the PVT temperature increases with φ; however, the slope of temperature enhancement is diminished with the increase in ṁ, and finally, at a maximum ṁ, the temperature is reduced by augmenting φ. At lower values of ṁ, less mass exchanges heat with the system. This amount of mass cannot cool the system. On the other hand, with the increase in φ for a constant ṁ, its ability to absorb heat decreases, reducing the PVT temperature. Although K of the NF is enhanced with φ, K enhancement cannot overcome the heat capacity reduction for low amounts of ṁ. One of the ways to compensate for the decrease in heat capacity is to increase ṁ and as a result, increase the heat transfer mass and fluid velocity so that K can spread the heat more uniformly and reduce the PVT temperature.

Figure 8a demonstrates that the maximum PVT temperature (319 K) corresponds to ṁ = 0.025 kg/s when the alumina/water concentration is 1 wt%, and the minimum one (307.96) corresponds to ṁ = 0.1 kg/s and φ = 1 wt%. Figure 8b shows different behavior for GNP/water. The PVT temperature has a decreasing trend with φ for a minimum ṁ (0.025 kg/s) by reaching φ = 0.25 wt% and then it enhances with a sharp slope. The decrease in PVT temperature continues by φ = 0.5 wt% for ṁ = 0.05 kg/s, and then, the PVT temperature increases with a gentler slope than that for ṁ = 0.025 kg/s. For ṁ =0.1 kg/s, the temperature has a decreasing trend. The maximum PVT temperature (319.62 K) corresponds to ṁ = 0.1 kg/s when the GNP/water concentration is 1 wt% and the minimum one (306.8 K) corresponds to ṁ = 0.1 kg/s and φ = 1 wt%. Figure 8c reveals that the PVT temperature has an increasing trend with φ for ṁ = 0.025 kg/s. For ṁ = 0.05 kg/s, the temperature is reduced with a slight slope; however, it enhances from φ = 0.5 wt% onwards. However, for ṁ = 0.1 kg/s, the PVT temperature has a descending trend. The maximum PVT temperature (319.11 K) corresponds to ṁ = 0.025 kg/s when the SiC/water concentration is 1 wt%, and the minimum one (307.55 K) corresponds to ṁ = 0.1 kg/s and φ = 1 wt%.

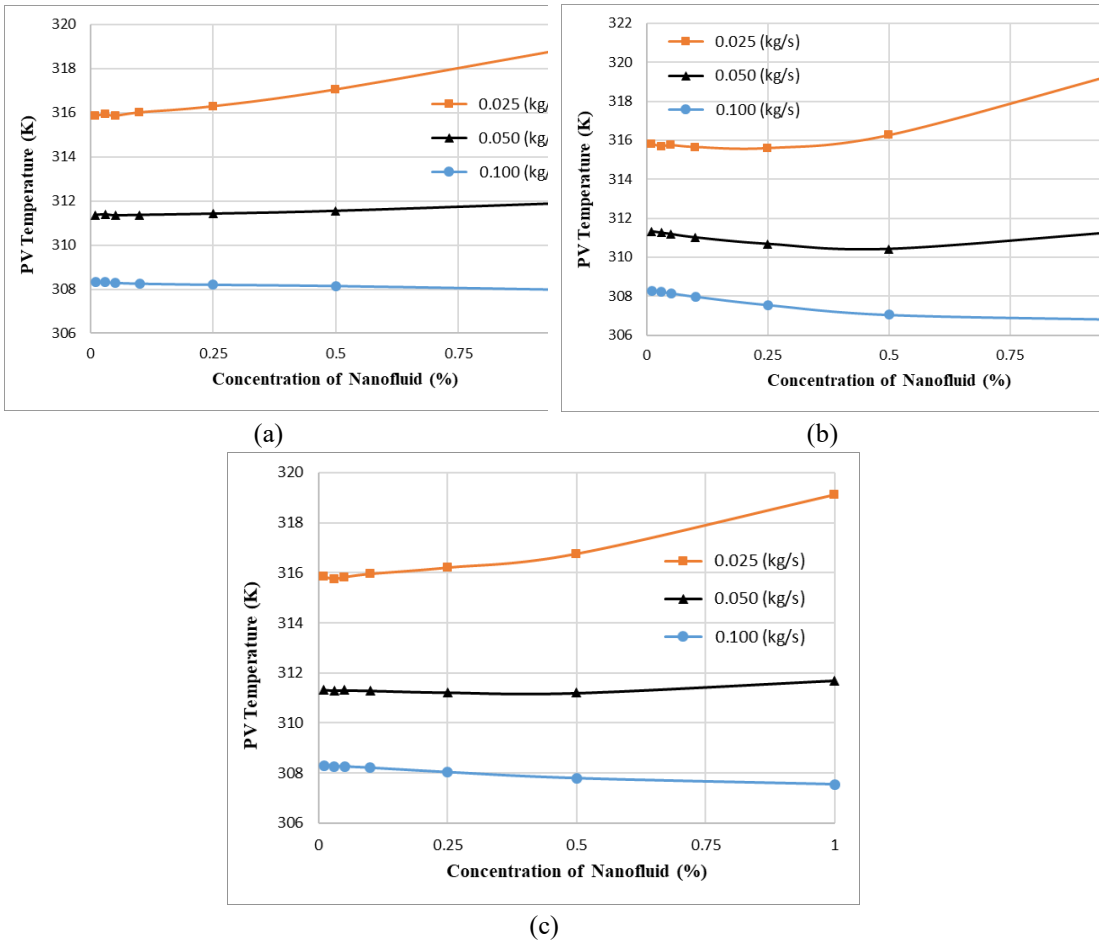

Figure 8. Effect of φ on PVT temperature for different amounts of ṁ: (a) alumina/water, (b) GNP/water, and (c) SiC/water.

Figure 9 shows the variations of η_{elec} with φ for different values of ṁ: 0.025, 0.05, and 0.1 kg/s. For low values of ṁ, $\eta_{elec}$is reduced with φ; however, for high values of ṁ, η_{elec} is improved with a gentle slope due to the decrease in PVT temperature. Figure 9a demonstrates that the maximum (14.33%) and minimum (13.58%) electrical efficiencies correspond to ṁ = 0.1 kg/s and 0.025 kg/s when the alumina/water is used. Figure 9b shows that for a minimum ṁ, there is a slight enhancement in $\eta_{elec}$with the increase in GNP/water concentration; however, it gradually declines for φ > 0.25 wt%. The primary enhancement in η_{elec} continues a little more for ṁ = 0.055 kg/s and it decreases with a slight slope for φ greater than 0.5 wt%. However, for ṁ = 0.1 kg/s, η_{elec} has an ascending trend for all amounts of φ. The behavior of η_{elec} depends on the PVT temperature. The maximum (14.41%) and minimum (13.54%) electrical efficiencies correspond to ṁv = 0.1 kg/s and 0.025 kg/s when the GNP/water is used. Figure 9c demonstrates that for ṁ = 0.025 kg/s, η_{elec} is reduced with φ. For ṁ = 0.05 kg/s, η_{elec} is enhanced and then reduced slightly. For ṁ = 0.1 kg/s, η_{elec} has a reducing trend. The maximum (14.35%) and minimum (13.57%) η_{elec} correspond to ṁ = 0.1 kg/s and 0.025 kg/s when the SiC/water is used.

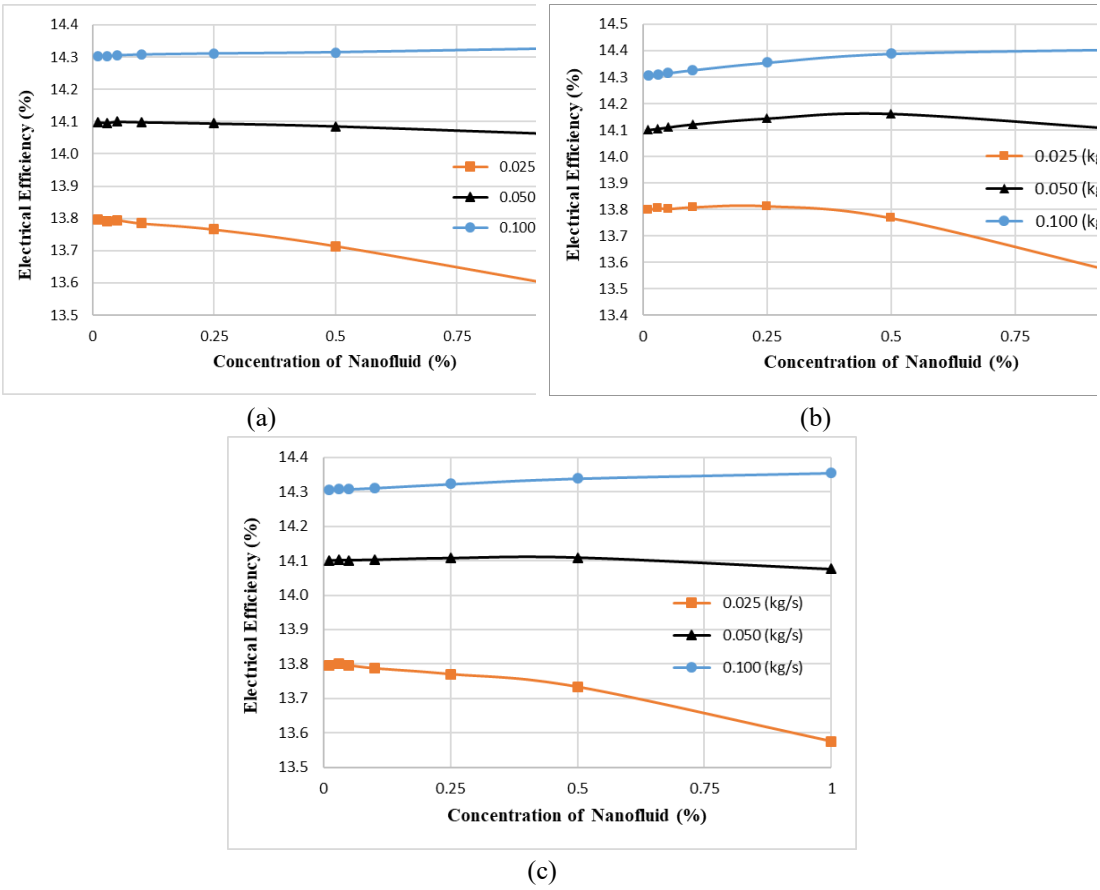

Figure 9. Effect of φ on η_{elec} of PVT for different values of ṁ: (a) alumina/water, (b) GNP/water, and (c) SiC/water.

Figure 10 shows the changes in η_{tot} in terms of φ for three amounts of ṁ. This figure shows the decreasing trend of η_{tot} for all amounts of ṁ due to the decrease in η_{th} and η_{elec}. Although for ṁ = 0.1 kg/s, η_{elec} has an ascending trend; this increase is insignificant compared to the decrease in η_{th}. Figure 10a illustrates that the maximum η_{th} (90.59%) corresponds to ṁ = 0.1 kg/s when the alumina/water concentration is 0.01 wt%, and the minimum one (59.79%) is related to ṁ = 0.025 kg/s and φ = 1 wt%. Figure 10b shows that the maximum η_{th} (90.58%) corresponds to ṁ = 0.1 kg/s when the GNP/water concentration is 0.01 wt%, and the minimum one (58.27%) is related to ṁ = 0.025 kg/s and φ = 1 wt%. Figure 10c demonstrates that the maximum η_{th} (90.58%) corresponds to ṁ = 0.1 kg/s when the SiC/water concentration is 0.01 wt%, and the minimum one (59.19%) is related to ṁ = 0.025 kg/s and φ = 1 wt%.

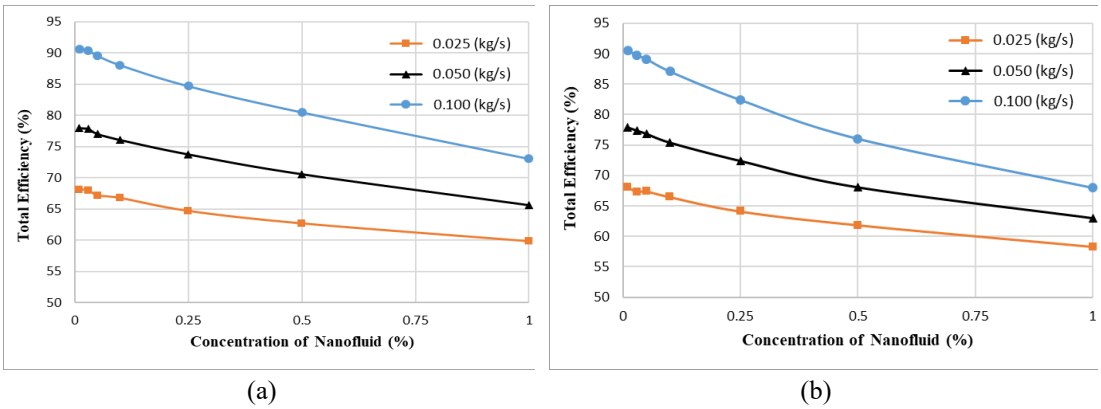

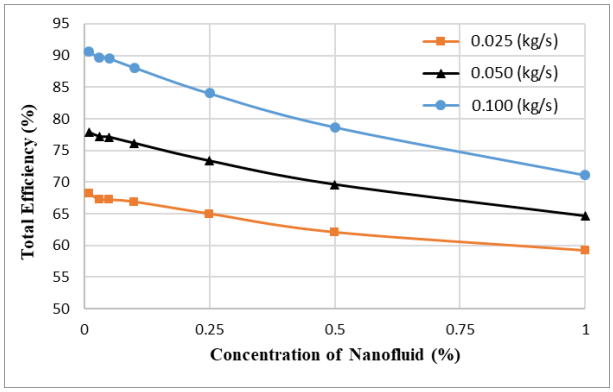

(c)

Figure 10. Effect of φ on η_{tot} of the PVT for different values of ṁ: (a) alumina/water, (b) GNP/water, and (c) SiC/water.

6.4. Effect of the inlet temperature

In this section, the performance of PVT system with and without fins is assessed for 0.5 wt% GNP/water NF and different inlet temperatures. In this study, the system with the number of fins 400 was used. Figure 11a illustrates T_{out} changes in terms of inlet temperature for a PVT system with and without fins. The outlet fluid temperature is enhanced with the fluid inlet temperature for both cases; however, this increase for the system without fins is greater than that for the system with fins. Therefore, the maximum T_{out} (349.91 K) corresponds to the system without fins at the inlet temperature of 348 K and the minimum value (301.53 K) corresponds to the system with fins at a temperature of 298 K. It should be noted that as the fluid inlet temperature increases, the temperature difference between the system and the environment increases, and this causes more heat to be transferred from the fins to the environment. Figure 11b presents the PVT temperature in terms of inlet temperature for PVT systems with and without fins. The PVT temperature increases as the inlet temperature increases for both systems; however, the difference between the values of the PVT temperature of the two systems is enhanced with the increase of the inlet temperature. The maximum PVT temperature (352.04 K) corresponds to the system without fins at the inlet temperature of 348 K and the minimum value (304.65) corresponds to the system with fins at a temperature of 298 K. Figure 11c illustrates the changes in η_{elec} of the system in terms of the inlet temperature for PVT systems with and without fins.

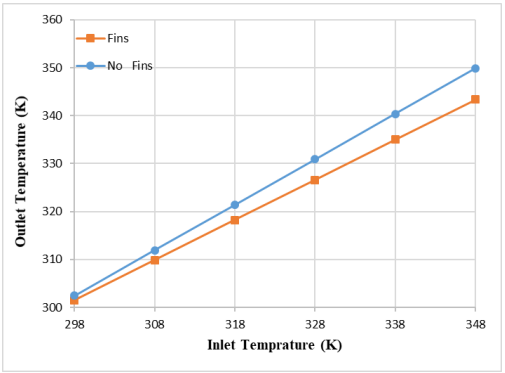

(a)

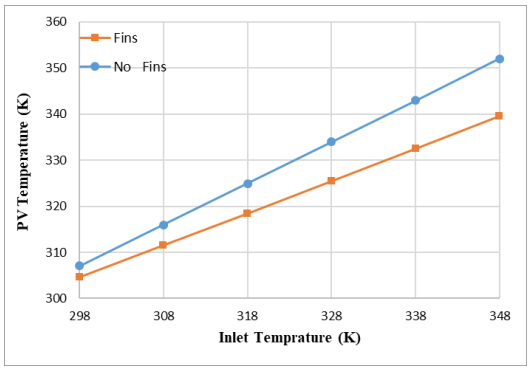

(b)

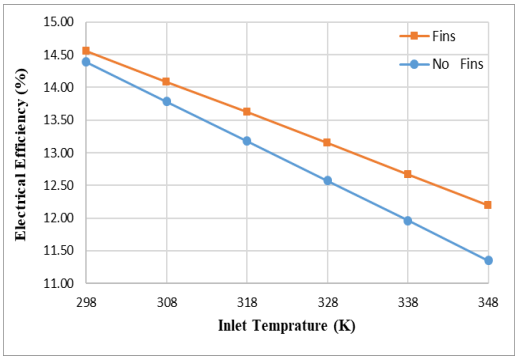

(c)

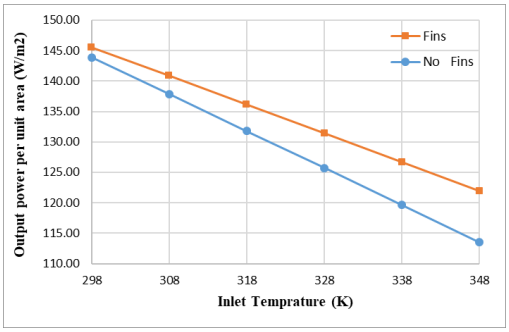

(d)

Figure 11. Effect of fluid inlet temperatures for two PVT systems with and without fins on (a) T_{out}, (b) PVT temperature, (c) electrical efficiency, and (d) output power.

It is observed that the slope variation of η_{elec} of the system without fins is lower than that of the case with fins because of higher PVT temperature due to less heat exchange with the environment. The maximum η_{elec} (14.55%) corresponds to the system with fins at the inlet temperature of 348 K and the minimum value (11.35%) corresponds to the system without fins at a temperature of 298 K. Figure 11d shows the system output power changes in terms of inlet temperature for PVT systems with and without fins, indicating a descending trend. The minimum output power for the system without fins is 113.52 W/m^2 which corresponds to 348 K and the maximum value for the system with fins 145.51 W/m^2 which corresponds to 298 K.

6.5. Effect of the solar radiation

This section examines the effect of SRI on the performance of the PVT systems with and without fins using a 0.5 wt% GNP/water NF. Figure 12a demonstrates the changes in T_{out} with solar radiation, showing that T_{out} is enhanced with solar radiation. The system without fins has a higher temperature than the system with fins because the fins cause part of the heat of the system to be transferred to the environment. The maximum (302.4 K) and minimum (298.71 K) values of T_{out} correspond to the system without fins with the maximum SRI and the system with fins with the minimum solar radiation, respectively. Figure 12b shows the difference between T_{in} and T_{out} by changing solar radiation. The ascending trend is observed for both systems. This figure shows the effect of absorbed heat on the temperature enhancement. The maximum (4.25 K) and minimum (0.56 K) temperature differences of the fluid inlet and outlet correspond to the systems with and without fins, respectively, when SRIv is 1000 W/m^2 and 200 W/m^2. Figure 12c illustrates the changes in PVT temperature in terms of solar radiation, indicating that the PVT temperature has an ascending trend for both systems with the increase of solar radiation. Due to heat transfer between fins and the environment, the system with fins has a lower PVT temperature than the system without fins. The maximum PVT temperature (307.05 K) corresponds to the system without fins when SRI is 1000 W/m^2, and the minimum temperature (299.34 K) corresponds to the system with fins when the radiation is 200 W/m^2. As SRI is enhanced, the temperature difference of the panel for the system with fins and without fins increases, which is because the system temperature increases with the solar radiation. Figure 12d demonstrates the changes in η_{elec} versus solar radiation. Since η_{elec} has an inverse relationship with the PVT temperature, $\eta_{elec}$is reduced with SRI due to the increase in the PVT temperature. The maximum η_{elec} (14.91%) is related to the system with fins when SRI is 200 W/m^2, and the minimum value (14.39%) is related to the system without fins when SRI is 1000 W/m^2. Figure 12e reveals the changes in output power versus solar radiation. With the increase of solar radiation, the output power is enhanced. Using fins does not affect the output power when SRI is low.

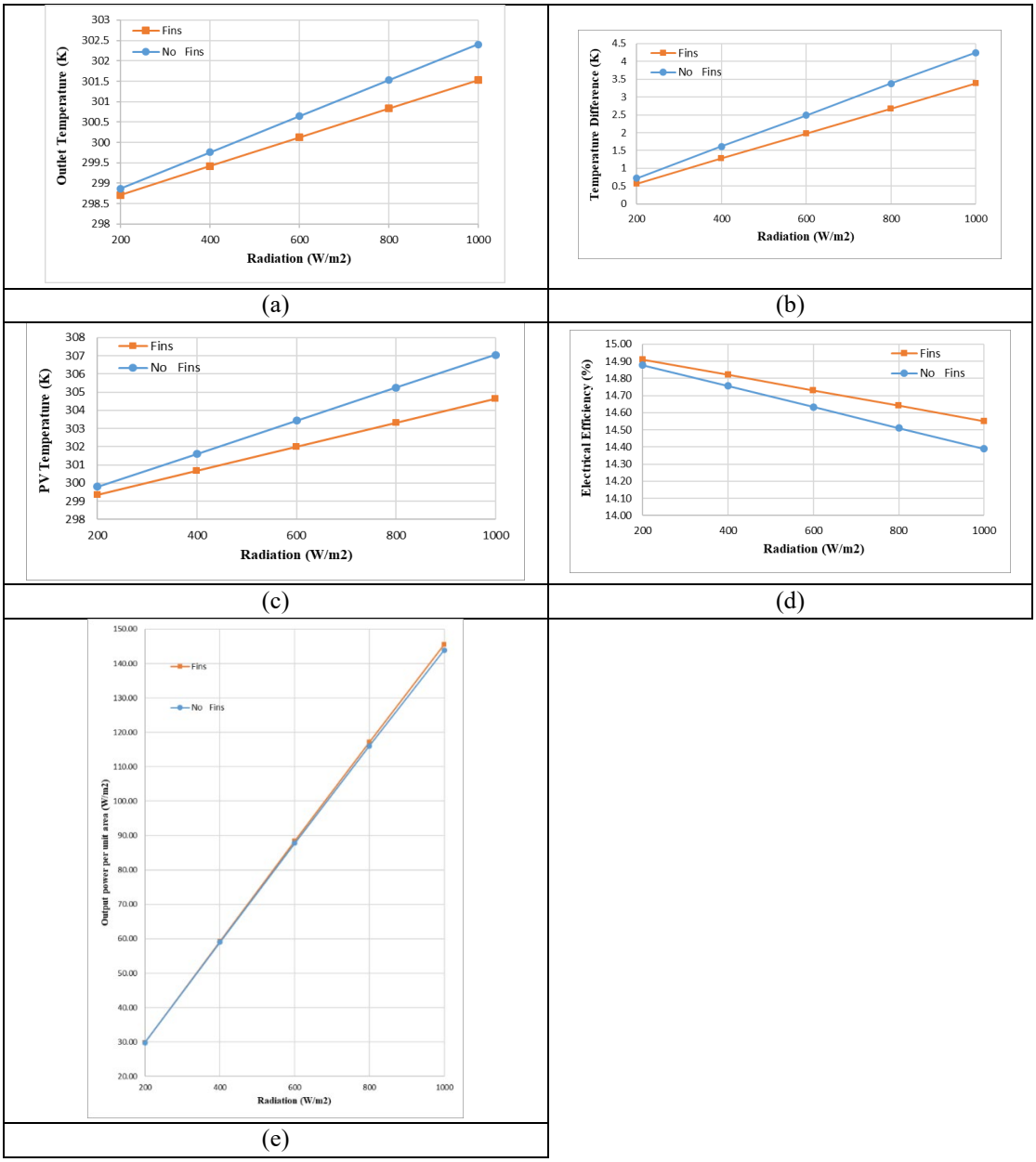

Figure 12. Effect of SRI on (a) T_{out}, (b) the temperature difference between the fluid inlet and outlet, (c) PVT temperature, (d) electrical efficiency, and (e) output power.

Eventually, the limitations of the present problem are expressed. Despite its creative potential, the study of parametric analysis of thermal and electrical performance of PVT systems employing nano-graphene coolants and improved fin design has a number of drawbacks. Although nano-graphene coolants provide better heat conductivity, they may eventually experience stability problems like sedimentation and agglomeration, as well as possible material compatibility and corrosion issues in the system. Furthermore, it is unclear how using graphene-based nanofluids will affect the environment and human health, and the high cost of manufacturing these nanomaterials makes their widespread use economically unfeasible. Improved fin designs can improve heat transmission, but they can also make production more difficult and expensive. The advantages might be small and rely on certain operating circumstances. There is a dearth of long-term performance data on such systems, and the majority of studies rely on controlled laboratory settings or simulations, which might not adequately represent the variable conditions found in real-world applications. Furthermore, before these technologies can be widely used, practical issues like field durability, maintenance, environmental regulation, and system integration must be resolved. Overall, even though the suggested techniques appear to have potential for increasing PVT system efficiency, substantial research and development work is required to get past obstacles related to technology, finances, and the environment before they can be used in a practical and

long-lasting manner.

7. Conclusions

This study simulates an NF-based PVT system featuring parallel tubes with fins positioned behind the heat absorber. The investigation assesses the effects of various parameters, including fin thickness, the number of fins, ṁ, types of NFs, φ, inlet temperatures, and SRI on the system's performance. The key findings of this research are as follows:

1. Fin thickness has minimal impact on PVT system performance; however, increasing the number of fins reduces T_{out}, η_{th}, and PVT temperature, while enhancing η_{elec}, and output power.
2. Increasing alumina nanoparticle concentration raises both outlet and PVT temperatures, yet it negatively affects η_{th}, η_{elec} , and η_{tot} .
3. An increase in ṁ of alumina/water NF lowers the PVT temperature while improving thermal, electrical, and overall efficiencies.
4. For GNP/water and SiC/water NFs, higher values of φ increase T_{out}, whereas a higher mass flow rate has a reverse impact.
5. PVT temperature and η_{elec} exhibit variable behavior with changes in ṁ, depending on φ.
6. Higher GNP/water and SiC/water concentrations decrease thermal and total efficiencies, while increased ṁ enhance these metrics.
7. For GNP/water NF, the highest T_{out} (316.83 K) occurs when ṁ = 0.025 kg/s and φ = 1 wt%; the lowest (301.68 K) occurs at 0.1 kg/s and φ = 0.01 wt%.
8. The highest PVT temperature (319.62 K) is observed for ṁ = 0.1 kg/s and φ = 1 wt%, while the lowest (306.8 K) corresponds to the same ṁ but with φ = 1 wt%.
9. The maximum η_{elec} (14.41%) is recorded when ṁ = 0.1 kg/s, while the minimum (13.54%) occurs at 0.025 kg/s using GNP/water.
10. The highest η_{elec} (14.55%) is achieved with fins at an inlet temperature of 348 K, whereas the lowest (11.35%) occurs without fins at 298 K, using 0.5 wt% GNP/water NF.

By preserving lower PV cell temperatures and boosting thermal energy collection, such cutting-edge cooling strategies may be practically included in hybrid renewable energy systems, solar farms, and building-integrated PVT systems to increase total energy production. Because of its excellent thermal conductivity, nano-graphene may be used as a coolant to greatly enhance the effectiveness of heat transfer. Additionally, optimized fin designs increase the surface area available for heat dissipation, which makes the system more efficient in a variety of climatic situations. Prototype testing under actual sun irradiation and various climatic circumstances may be part of future experimental validation to measure gains in thermal energy recovery and electricity output.

Nomenclature

A_c	Collector surface area (m^2)	T_r	Cell reference temperature (K)
A_{pv}	PVT surface area (m^2)	Q_u	Thermal energy (J)
C_p	Specific heat capacity (J/kg. K)	u, v, w	Velocity components (m/s)
E_{pv}	Electric power output (W)	V_{wind}	Wind speed (m/s)
g	Gravity acceleration (m/s^2)	**Greek letters**	
G	Incident solar radiation (J/m^2)	β	Volume expansion coefficient (1/K)
h	Convective heat transfer coefficient ($W/m^2.K$)	ρ	Density (kg/m^3)
K	Thermal conductivity (W/m.K)	μ	Dynamic viscosity (Pa.s)
ṁ	Mass flow rate (kg/s)	η_{elec}	Electrical efficiency (%)
p	Pressure (Pa)	η_r	PVT efficiency (%)
T_{in}, T_{out}	Fluid inlet and outlet temperature (K)	η_{th}	Thermal efficiency (%)
T_{cell}	PV cell temperature (K)	η_{tot}	Total efficiency (%)

References

Abdallah SR, Elsemary IMM, Altohamy AA, Abdelrahman MA, Attia AAA, Abdellatif OE (2018) 'Experimental investigation on the effect of using nano fluid (Al2O3-Water) on the performance of PV/T system', Thermal Science and Engineering Progress, 7, pp. 1-7. Available at: https://doi.org/10.1016/j.tsep.2018.06.008

Ahmed A, Fouda A, Elattar HF, Alnasami K, Alsharif AMA (2025) 'Advancing photovoltaic thermal module efficiency through optimized heat sink designs', Applied Thermal Engineering, 271, p. 126241. Available at: https://doi.org/10.1016/j.applthermaleng.2025.126241

Al-Shamani AN, Alghoul MA, Elbreki AM, Ammar AA, Abed AM, Sopian K (2018) 'Mathematical and experimental evaluation of thermal and electrical efficiency of PV/T collector using different water based nano-fluids', Energy, 145, pp. 770-792. Available at: https://doi.org/10.1016/j.energy.2017.12.041

Al-Waeli AHA, Sopian K, Chaichan MT, Kazem HA, Hasan HA, Al-Shamani AN (2017) 'An experimental investigation of SiC nanofluid as a base-fluid for a photovoltaic thermal PV/T system', Energy Conversion and Management, 142, pp. 547-558. Available at: https://doi.org/10.1016/j.enconman.2017.03.009

Alhamayani A (2024) 'Numerical analysis and deep learning algorithm for photovoltaic-thermal systems using various nanofluids and volume fractions at Riyadh, Saudi Arabia', Case Studies in Thermal Engineering, 54, p. 103974. Available at: https://doi.org/10.1016/j.csite.2024.103974

Alktranee M, Al-Yasiri Q, Shehab MA, Bencs P, Németh Z, Hernadi K (2024) 'Experimental and numerical study of a photovoltaic/thermal system cooled by metal oxide nanofluids', Alexandria Engineering Journal, 94, pp. 55-67. Available at: https://doi.org/10.1016/j.aej.2024.01.007

Arifin Z, Prasetyo SD, Tjahjana DDDP, Rachmanto RA, Prabowo AR, Alfaiz NF (2022) 'The application of TiO2 nanofluids in photovoltaic thermal collector systems', Energy Reports, 8, pp. 1371-1380. Available at: https://doi.org/10.1016/j.egyr.2022.03.021

Chandan V, Suresh V, Iqbal SM, Reddy KS, Pesala B (2021) '3-D numerical modelling and experimental investigation of coupled photovoltaic thermal and flat plate collector', Solar Energy, 224, pp. 195-209. Available at: https://doi.org/10.1016/j.solener.2021.07.054

Hai T, Abidi A, Wang L, Abed AM, Mahmoud MZ, Tag El Din EM, Smaisim GF (2022) 'Simulation of solar thermal panel systems with nanofluid flow and PCM for energy consumption management of buildings', Journal of Building Engineering, 58, p. 104981. Available at: https://doi.org/10.1016/j.jobe.2022.104981

Hakimi M, Baniasadi E, Afshari E (2024) 'A comparative study on novel active cooling and heat recovery techniques for photovoltaic-thermal collectors', Process Safety and Environmental Protection, 190, pp. 1233-1252. Available at: https://doi.org/10.1016/j.psep.2024.03.045

Hasan HA, Hatem AA, Abd LA, Abed AM, Sopian K (2022) 'Numerical investigation of nanofluids comprising different metal oxide nanoparticles for cooling concentration photovoltaic thermal CPVT', Clean Engineering and Technology, 10, p. 100543. Available at: https://doi.org/10.1016/j.clet.2022.100543

Khodadadi M, Farshad SA, Ebrahimpour Z, Sheikholeslami M (2021) 'Thermal performance of nanofluid with employing of NEPCM in a PVT-LFR system', Sustainable Energy Technologies and Assessments, 47, p. 101340. Available at: https://doi.org/10.1016/j.seta.2021.101340

Khan SY, Liu S, Kumar M, Mazhar AR, et al. (2024) 'Data analysis and review of the research landscape in performance-enhancing thermal management strategies of photovoltaic technology', Sustainable Energy Technologies and Assessments, 70, p. 103938. Available at: https://doi.org/10.1016/j.seta.2024.103938

Lari MO, Sahin AZ (2017) 'Design, performance and economic analysis of a nanofluid-based photovoltaic/thermal system for residential applications', Energy Conversion and Management, 149, pp. 467-484. Available at: https://doi.org/10.1016/j.enconman.2017.05.002

Maadi SR, Khatibi M, Ebrahimnia-Bajestan E, Wood D (2019) 'Coupled thermal-optical numerical modeling of PV/T module – Combining CFD approach and two-band radiation DO model', Energy Conversion and Management, 198, p. 111781. Available at: https://doi.org/10.1016/j.enconman.2019.111781

Maadi SR, Navegi A, Solomin E, Ahn HS, Wongwises S, Mahian O (2021) 'Performance improvement of a photovoltaic-thermal system using a wavy-strip insert with and without nanofluid', Energy, 234, p. 121190. Available at: https://doi.org/10.1016/j.energy.2021.121190

Nasrin R, Rahim NA, Fayaz H, Hasanuzzaman M (2018) 'Water/MWCNT nanofluid based cooling system of PVT: Experimental and numerical research', Renewable Energy, 121, pp. 286-300. Available at: https://doi.org/10.1016/j.renene.2018.01.102

Oztürk M, Yüksel C, Çiftçi E (2024) 'Energy, exergy and sustainability analysis of a photovoltaic-thermal solar system with nano-enhancement and thermal energy storage integration', Process Safety and Environmental Protection, 187, pp. 593–604. Available at: https://doi.org/10.1016/j.psep.2023.10.009

Rajvikram M, Sivasankar G (2019) 'Experimental study conducted for the identification of best heat absorption and dissipation methodology in solar photovoltaic panel', Solar Energy, 193, pp. 283-292. Available at: https://doi.org/10.1016/j.solener.2019.09.022

Shehadeh SH, Aly HH, El-Hawary ME (2019) 'Investigation of photovoltaic coverage ratio for maximum overall thermal energy of photovoltaic thermal system', Renewable Energy, 134, pp. 757-768. Available at: https://doi.org/10.1016/j.renene.2018.11.061

Sofiah AGN, Rajamony RK, Samykano M, Pande AK, Pasupuleti J, Sulaiman NF (2024) 'Assessment on thermophysical properties of nano enhanced heat transfer fluid with hexagonal boron nitride nanoparticles for thermal management of photovoltaic thermal (PVT) system', Process Safety and Environmental Protection, 189, pp. 1087-1102. Available at: https://doi.org/10.1016/j.psep.2023.12.065

Sreekumar S, Shah N, Mondol JD, Hewitt N, Chakrabarti S (2022) 'Numerical investigation and feasibility study on MXene/water nanofluid based photovoltaic/thermal system', Clean Energy Systems, 2, p. 100010. Available at: https://doi.org/10.1016/j.cesys.2022.100010

Sreekumar S, Shaji J, Cherian G, Thomas S, Mondol JD, Shah N (2024) 'Corrosion analysis and performance investigation of hybrid MXene/C-dot Nanofluid-Based direct absorption solar collector', Solar Energy, 269, p. 112317. Available at: https://doi.org/10.1016/j.solener.2023.112317

Yazdanifard F, Ebrahimnia-Bajestan E, Ameri M (2016) 'Investigating the performance of a water-based photovoltaic/thermal (PV/T) collector in laminar and turbulent flow regime', Renewable Energy, 99, pp. 295-306. Available at: https://doi.org/10.1016/j.renene.2016.01.034